Surface-Defect-Mediated Channel for Oxygen Incorporation into Ru(0001)†

R. Blume and H. Niehus

Institut für Physik, Humboldt-Universität zu Berlin, Newtonstrasse 15, 12489 Berlin, Germany

H. Conrad

Fritz-Haber-Institut der Max-Planck-Gesellschaft, Faradayweg 4-6, 14165 Berlin, Germany

A. Böttcher*

Institut für Physikalische Chemie, Universität Karlsruhe (TH), Kaiserstrasse 12, 76131 Karlsruhe, Germany

Received: January 7, 2004; In Final Form: March 24, 2004

The capacity of intentionally created defects to act as possible channels for oxygen incorporation into the subsurface region has been studied by means of thermal desorption spectroscopy and ultraviolet photoelectron spectroscopy (21.2 eV). Thermal-energy atom scattering has been applied to determine the overall surface roughness as achieved by exposing the surface to a flux of low-energy Ar^+ ions. Within a wide range of experimental conditions the low-temperature ($T \leq 600$ K) and high-pressure ($p \approx 1$ bar) oxidation regime applied here does not lead to a significant formation of bulk oxides. Instead two competing channels for oxygen incorporation into the subsurface region have been identified. The first path proceeds via the penetration of the oxygen monolayer adsorbed on top of the defect-free surface areas. The second path is defect-mediated and exhibits a maximum capacity of about 10 oxygen atoms per defect. This reaction channel is thermally activated with an apparent activation energy of 0.15 eV, which is nearly 3 times lower than the activation energy corresponding to the growth of oxide domains.

1. Introduction

Surface imperfections were often simply ignored in surface science as an inconvenient minority species which interferes with the idea of an ideal surface as a physical system. Today surface defects represent an issue of fundamental technological as well as scientific importance. There are numerous interesting aspects intensely studied these days by applying sensitive techniques of modern surface science.[1]

It is well established that metal atoms or clusters as mobile adsorbed species are pinned by surface imperfections, defects, and steps existing even at the smoothest surfaces.[2] They act as traps for cluster and adsorbates. Their unique electronic properties drive further nucleus formation and growth of the adsorbed phase.[3] The associated electron transfer resulting from the defect−cluster interaction is size-selective, and modifies considerably the overall reactivity of pinned clusters.[4]

An extensive scanning tunneling microscopy (STM) study of hydrogen adsorption on Pd(111) indicates that adjacent dimer vacancies are never active sites for H_2 dissociation.[5] This rather surprising finding sheds light on the dynamics of the chemisorptive event and stresses the chemisorption-induced mobility of a surface vacancy. The chemical role of surface defects became evident by measurements of the initial probability for dissociative oxygen chemisorption on Cu(100).[6] Steric blocking of the surface defects by various adsorbates resulted in a considerable reduction of the initial sticking coefficient.

Recently, surface defects have attracted attention as possible channels opened for thermally driven incorporation and intercalation of impurity atoms into the subsurface region. For example, a comparative theoretical study suggests a path for carbon incorporation into the Si(001) surface based on the lowering of the activation barrier offered by embedded dimer vacancies.[7] Further, the oxygen storage capacity of catalysts has been recognized as an important feature limiting the yield of numerous chemical reactions.[8] For instance, ceria−zirconia catalysts decorated with noble-metal particles exhibit two channels for oxygen storage: oxygen is associated with deposited metal particles as well as incorporated into the outermost layers of the oxide surface. Interestingly, the oxygen load associated with metal particles as minority species reached about 50% of the total oxygen amount stored.

Our recent study of oxygen incorporation into smooth Ru(0001) surfaces revealed a considerable capacity of these surfaces toward oxygen storage in the subsurface region.[9] It was possible to incorporate more than 4 monolayer equivalents (MLEs) of oxygen in the subsurface region without any traces of bulk oxides. However, the presence of residual defects and surface imperfections could not be entirely excluded even after extended annealing procedures were performed, and consequently, the role of surface defects in the oxygen incorporation process still remains an open question.

To clarify the role of intentionally created defects in oxygen incorporation into Ru(0001), we applied thermal desorption spectroscopy (TDS), ultraviolet photoelectron spectroscopy (UPS), low-energy electron diffraction (LEED), and the scattering of a thermal-energetic supersonic He beam (TEAS).[10] The oxidation procedure chosen here is identical to that applied previously to study oxygen incorporation into a smooth surface.[9] It is based on a low-temperature and high-pressure (LTHP)

† Part of the special issue "Gerhard Ertl Festschrift".

* To whom correspondence should be addressed. E-mail: artur.boettcher@chemie.uni-karlsruhe.de.

10.1021/jp0400059 CCC: $27.50
Published on Web 07/17/2004

surface exposure to oxygen, which ensures an oxide-free oxygen incorporation into the subsurface. The capacity of the surface to accumulate oxygen has been found to be considerably increased by the presence of defects. In fact, the process of defect-mediated oxygen uptake represents the dominating reaction channel. The apparent activation barrier for the defect-mediated incorporation channel is 3 times smaller than the activation barrier found for the formation of bulk oxides.[11] Moreover, the formation of oxide domains at a defect-rich surface starts at significantly larger oxygen exposures than that measured for smooth surfaces. The TDS- and UPS-based studies result in a state diagram for the defect-associated oxygen accumulation. It clearly defines the space of parameters where the oxygen incorporation proceeds without the formation of bulk oxides.

2. Experimental Section

All experiments were conducted in a UHV chamber at a base pressure lower than 5×10^{-10} mbar. The chamber was equipped with standard facilities for sample cleaning and sputtering as well as for sample characterization (LEED/Auger electron spectroscopy (AES), TDS, and UPS (21.2 eV)). The analytical chamber was connected to a molecular beam apparatus which enabled the scattering of thermal He atoms (TEAS). The main vacuum system has been designed to perform high oxygen exposures at partial pressures up to 1 bar. This setup provided a quick oxygen evacuation reaching UHV conditions ($p < 10^{-9}$ mbar) within 15 min.

The Ru(0001) crystal has been cleaned by sequenced cycles of Ar^+ sputtering (2 kV, 3−10 μA for 10 min) and annealing to 1550 K.[12,13] The cleanliness of the surface has been checked by UPS and AES.

Surface imperfections have been created by exposing the clean and smooth surface to a weak flux of low-energy Ar^+ ions (500 eV, 0.7 μA). Note that the sputtering procedure has been applied only when the preceding He scattering in the specular direction revealed a maximum of surface smoothness. The TEAS-based roughness determination stems from the fact that adsorbed atoms and surface defects effectively reduce the intensity of the primary beam in the specular direction. This leads to a considerable angular redistribution of the scattered atoms over the whole half-space. Thus, the resulting surface roughness has been determined by measuring the He flux scattered from the sputtered, I_{rough}, and smooth, I_{smooth}, surfaces. Subsequently, the so-called mean surface roughness, $\rho = (I_{smooth} - I_{rough})/I_{smooth}$, has been estimated and used as a simple measure of the mean surface topography. The reference intensity, I_{smooth}, has been determined after repeated heating to 1550 K until the maximum of He reflectivity, $I_{smooth} = I_{max}$, was reached. Further heating cycles did not change the maximum value and consequently signaled the state of the smoothest surface achievable.

The oxygen incorporation into the ruthenium surface has been performed by exposing the sample to high-purity molecular oxygen at constant partial pressures ranging from 10^{-9} mbar to 1 bar. The oxygen exposure was started only after a fixed sample temperature was reached, which was monitored and stabilized by a K-type thermocouple spot welded to the backside of the crystal. The partial pressure was controlled by using the IKR060 and TPR018 instruments (Balzers) for pressures below and above 10^{-3} mbar, respectively. Thermal desorption spectra were taken by applying resistive heating to the sample with a constant heating rate of 4 K/s. The oxygen load of the Ru sample was determined by integrating the O_2 TD traces of the leaving oxygen. The resulting areas were calibrated by combining the corresponding LEED and TDS data of a saturated adsorbed oxygen layer ($\Theta = 1$) which forms a (1×1)-O LEED superstructure.[30] The oxygen coverage is then expressed in terms of MLEs (1 MLE = 1.58×10^{15} cm^{-2}).

After the crystal was heated to 1550 K oxygen traces could be detected neither by TDS nor by UPS and AES. Similarly, the He reflectivity reached the highest level already after subsequent heating cycles were performed. Nevertheless, to avoid a possible oxygen-induced long-term degradation of the subsurface region by oxygen accumulation in deeper located bulk regions, every new oxidation procedure was started only after extended sputtering and annealing cycles were performed.

3. Results

A. Characterization of a Defect-Rich Surface. Prior to discussing the announced role of surface defects in the oxygen incorporation process, we present a brief analysis of the roughness of the sputtered surfaces. The aim was to create surface defects as species only slightly disturbing the still intact surface. Obviously, a gentle sputtering procedure has been applied to avoid a possible long-range destruction of the surface periodicity. The time evolution of the mean surface roughness $\rho(t)$ as measured by He scattering after the Ar^+ sputtering was performed ($E_{kin} = 500$ eV) represents a monotonic function increasing with the sputtering time. It starts to saturate already after $t \approx 75$ s and reaches a level of 0.4, which has been found to be the highest value achievable by using this procedure on Ru(0001). The time interval to reach saturation is shortened by increasing the impact energy, but the corresponding TEAS-derived mean roughness changes insignificantly even for energies around 2 keV ($\rho \approx 0.44$). This rather low value indicates that the sputtering procedure applied here does not result in a total disorder of the surface and deeper lying regions but suggests that the Ar^+ sputtering procedure leads solely to a partial removal of the topmost ruthenium layers. This finding is supported by recently performed model calculations as well as by secondary-ion mass spectrometry (SIMS) measurements.[13,14] It is well-known that the initial sputtering probability for Ar^+ ions impinging the Ru(0001) with kinetic energies lower than 1 keV is around 1.[15,16] However, the mean sputtering probability at a virgin smooth Ru(0001) surface is considerably reduced by the presence of defects already created; i.e., the removal probability for Ru atoms decreases gradually with progressing sputtering and levels off at a steady-state value of about 0.5 at an ion dose of 1.7×10^{15} cm^{-2}.[15] Thus, taking this probability decay into account, the overall amount of removed Ru atoms which results in the saturation of the mean roughness is estimated to be about 0.8 MLE. Moreover, it has been shown that for kinetic energies lower than 1 keV the mean depth of the destructed region extents solely over two outermost Ru layers, and the fraction of defected sites in the first layer is nearly 6 times higher than that found inside the second layer.[14] Consequently, when these findings are transferred to our sputtering conditions, the outermost Ru layer should contain still 0.3 MLE of the unperturbed areas and the second layer 0.9 MLE. Furthermore, the estimation of the cross section for Ru removal as derived from the SIMS measurements[15] implies that only four adjacent Ru atoms are involved in a successful sputtering event; i.e., the defects created represent rather individual Ru vacancies. In the following we will take this picture as a basis for further analysis. A more detailed analysis of the surface topography and the defect morphology remains outside the scope of this paper and would require a separate STM-based study.

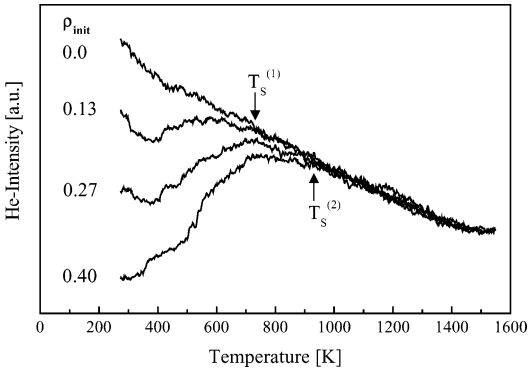

Figure 1. Evolution of the mean roughness as monitored by the He scattering technique applied during thermal annealing of the surface. Four examples are displayed differing by the initial roughness, ρ_{init}. $T_s^{(1)}$ indicates the temperature at which the roughness changes due to annihilation of first-layer defects. $T_s^{(2)}$ indicates the temperature at which the roughness reached a value characteristic for a smooth surface.

Figure 1 shows the annealing-induced evolution of the He flux, $I_{He}(T)$, scattered on surfaces differing by their initial mean roughness. The distinct initial mean roughness in the four examples shown here has been reached by exposing the clean smooth surface to different Ar^+ doses at the same impact energy. For a smooth surface (topmost curve, $\rho_{init} = 0$) a gradual decay of the He flux with increasing sample temperature mirrors the phonon-induced roughness as described by the Debye−Waller factor.[17] The sputtered surfaces exhibit a more complex thermal behavior which strongly depends on the Ar^+ dose applied. For short Ar^+ sputtering the subsequent annealing procedure leads to a distinct drop of the He flux ($\rho_{init} = 0.13$). It reaches a minimum around a sample temperature of 400 K, which can be attributed to a significant increase of the effective roughness. Individual Ru atoms can emerge from defect sites or defected step edges onto flat terraces. Such single atoms scatter He atoms more efficiently than Ru atoms embedded in a complete layer. For higher temperatures the scattered He flux increases, which indicates defect annihilation and a smoothing of step edges. This gradual renewal of the surface can be attributed to vacancy−adatom recombination due to the thermally activated migration of Ru adatoms.[18] The process seems to be completed at surface temperatures around 700 K (indicated as $T_s^{(1)}$). For surfaces with an initial mean roughness higher than about 0.2 the annealing curve $I_{He}(T)$ passes through two distinct stages. The first stage is similar to that observed for lower mean roughness and is again completed at $T_s^{(1)} = 700$ K, but it is accompanied by a larger increase of the corresponding He flux as expected for surfaces exhibiting a higher initial defect density. The subsequent second stage extents up to $T_s^{(2)} = 950$ K, where the slope of the $I_{He}(T)$ curve changes considerably. It does not reach the maximum value characteristic for a smooth surface. According to the model postulated above, for mean roughness between 0.18 and 0.4 also a significant damage of the second Ru layer has to be expected.[15] Thus, the second stage in the annealing curve $I_{He}(T)$ can be assigned to some smoothing and annihilation processes concerning the second Ru layer. Finally, at temperatures of about 950 K, the healing of the surface is completed as indicated by $I_{He}(T)$, which reaches the value characteristic for a smooth surface. It has to be mentioned that surfaces sputtered with a kinetic energy of 2 keV again reached nearly perfect smoothness only at temperatures around 1500 K.

Summarizing this part, by combining our TEAS-based analysis and the SIMS-derived findings, the topography of the sputtered surface appears to be stamped by rather single-atom vacancies distributed over two outermost surface layers. The subsequent annihilation process is completed at surface temperatures below 900 K and consequently indicates that the sputtering procedure applied represents a rather gentle kind of surface defecting.

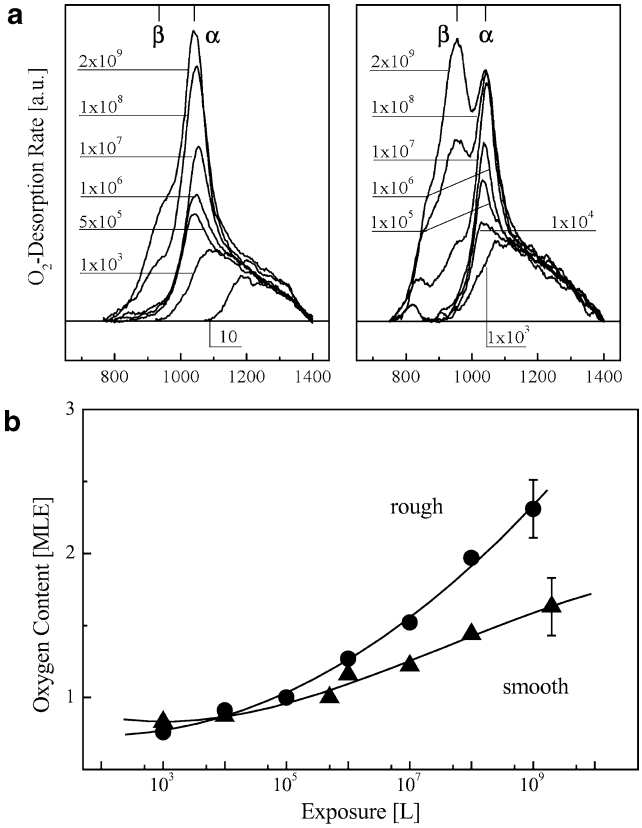

Figure 2. (a, top) O_2 TD spectra taken after exposure of the smooth and defect-rich surfaces to increasing oxygen amounts, left and right panels, respectively. The samples were kept at a constant temperature of 460 K. The rough surfaces exhibited a nearly identical mean roughness of 0.4. Note that the intensities displayed for a smooth and a defect-rich surface are not the same. (b, bottom) Oxygen load deposited on defect-rich and smooth surfaces achieved by exposure of the surfaces to increasing oxygen doses. The corresponding O_2 TD spectra are shown in (a).

B. Oxygen Incorporation into a Defect-Rich Surface. Figure 2a shows two series of O_2 TD spectra taken after the same sequence of oxygen exposures was performed at a sample temperature of 460 K on a smooth and a defect-rich Ru(0001) surface, left and right panels, respectively. The defect-rich surface exhibited an initial roughness of 0.4. Both O_2 TD series show three well-distinguishable spectral features. At oxygen doses lower than 10^5 L the corresponding TD spectra exhibit only a wide band originating from recombinative desorption from oxygen chemisorbed on the smooth areas of the surface. The temperature of the desorption onset shifts downward with increasing lateral density of chemisorbed atoms. This trend has been explained by a repulsive atom−atom interaction in the layer, which for reduced distances between adjacent adatoms considerably lowers the activation energy for desorption.[19,20] An additional TD peak, α, arises at 1040 K on both the smooth and defect-rich surfaces when the sample is exposed to oxygen doses higher than 10^5 L. This peak signals that the 2D oxygen layer becomes complete and an additional process of oxygen incorporation starts. Peak α was recently assigned to the thermal removal of subsurface oxygen deposited mainly between the two outermost Ru layers, Ru(I) and Ru(II).[9,21,22] The maximum capacity for oxygen incorporation for this channel was found to be about 0.6 MLE. The third peak, β, is located at 940 K.

On the smooth surface this peak is only detectable for exposures higher than 10^8 L, whereas on a defect-rich surface its growth starts already at an exposure of 10^7 L. It has been suggested that this peak might be attributed to a defect-mediated incorporation channel.[9] This rather preliminary interpretation is nicely supported here when the two panels in Figure 2a are compared. Whereas for the defect-poor surface the TD spectra exhibit solely a weak shoulder at 940 K even for exposures around 10^9 L, peak β is well-shaped and clearly distinguishable from the neighboring peak already for oxygen exposures of 10^8 L. The intensity of peak β increases continuously with progressing oxygen exposure. In contrast to this trend, the growth of peak α slows significantly beyond a dose of 10^9 L. In this stage peak α for the sputtered surface is only slightly lower than observed for the smooth surface. The O_2 TD spectra show clearly that the presence of intentionally created surface defects manifests itself mainly by peak β, which at this stage solely represents the defect-mediated desorption channel.

Figure 2b shows oxygen uptake curves as obtained by integrating the O_2 TD spectra shown in Figure 2a for smooth and rough surfaces. For oxygen exposures lower than 10^5 L, where the chemisorbed layer is gradually completed, the two curves remain undistinguishable within the error bars; i.e., the presence of surface defects affects the adlayer growth insignificantly. The role of surface defects becomes pronounced within later stages of oxygen exposure where oxygen atoms start to penetrate the subsurface region. The oxygen load deposited at the defect-rich surface is significantly higher than that measured at the smooth surface after exactly the same oxygen exposures are applied. After the surfaces were exposed to an oxygen dose of 10^9 L the difference already reached a value of about 0.7 MLE.

According to the experiments presented above, the role of surface defects becomes detectable only when a completed oxygen adlayer covers the surface. This result implies that the initial probability for dissociative sticking of impinging oxygen molecules is not significantly affected by the presence of surface defects within the error bars of our experiment. This finding is supported by recent molecular beam scattering experiments which revealed a probability for dissociative sticking of 0.4 ± 0.06 at room temperature for both the smooth and defect-rich surfaces.[11,23] Similar behavior has been observed by Hirsimäki and Chorkendorff[6] for the dissociative chemisorption of oxygen on Cu(100), where the presence of surface defects could not be reflected by measurements of the initial sticking probability. Thus, we can state here that the dissociative sticking coefficient is not the decisive factor for the observed differences in the uptake curves (Figure 2b). To appropriatly characterize the role of surface defects, the concept of mean incorporation probability is applied. This probability is calculated as the ratio between the total oxygen load deposited in the surface and the total number of impinging oxygen molecules on the surface during the exposure. For a smooth surface this value ranges from about 5×10^{-11} at 350 K to 10^{-10} at 600 K. Within the same temperature range the defect-rich surface exhibits 2 times higher incorporation probabilities on average. For instance, it reaches a value of 2×10^{-10} after the surface is exposed to 10^{11} L of oxygen at 600 K.

Figure 3 illustrates how the ratio of peak intensities, $\eta = C_\beta/C_\alpha$, calculated from fitted and subsequently integrated Gaussian profiles representing peaks α and β, evolves due to increasing oxygen exposures. It shows a representative example for all experiments we conducted within the temperature range up to 600 K (here $T = 500$ K). For both surfaces, $\rho = 0$ and $\rho = 0.4$, the ratio η increases with progressing oxygen exposure up to a dose of about 10^{10} L, where pronounced maxima are observed. In the presented case $\eta_{max} = 2$ and 18 have been found for the smooth and defect-rich surfaces, respectively. Beyond a critical dose $D^* \cong 10^{10}$ L the ratio drops with increasing exposures. Note that D^* depends on the preparation temperature. It becomes larger at lower sample temperatures; for instance, at 375 K it reaches a value of 10^{12} L. The maximum ratio η_{max} scales with the total defect density. The sharp bend in the curve $\eta(D)$ signals that the limited defect capacity becomes exhausted and the oxygen incorporation via defects slows considerably. Instead, a gradual increase of C_α is observed, which might indicate an interaction between the α and β channels. This aspect will be analyzed in detail in the Discussion.

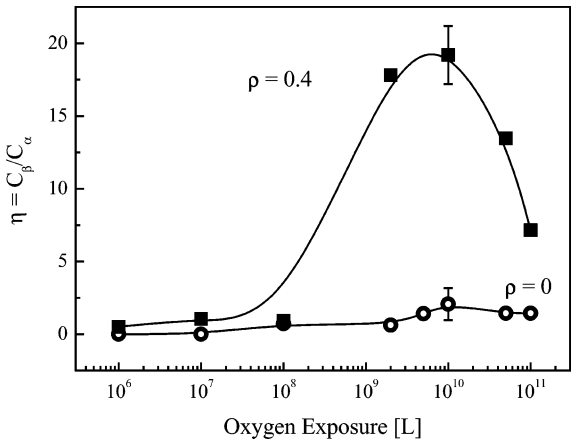

Figure 3. Evolution of the ratio $\eta = C_\beta/C_\alpha$ induced by increasing the oxygen exposure applied to a smooth (○) and a defect-rich (■) surface at the same sample temperature of 500 K (C_β denotes the oxygen load incorporated via surface defects, and C_α represents the oxygen amount deposited via channel α).

When the basis of O_2 TDS is strictly considered, the pronounced peak β may represent solely a desorption channel. This peak cannot be a priori related to the surface-defect-mediated channel for oxygen incorporation without additional experimental hints. However, the main finding derived from the experiment presented above, C(defect-rich) > C(smooth) (Figure 2b), clearly indicates an additional role of surface defects. They can be considered as active channels for oxygen dissolution as well.

To find an electronic marker of the oxygen species associated with the adsorption−desorption channel β, we analyze the valence band of the smooth and sputtered surfaces before and after exposing it to large oxygen doses. Spectra of clean smooth surfaces show three pronounced features at binding energies of 0.4, 2.4, and about 5 eV.[23,24] Interestingly, the spectrum of a clean (not oxidized), defect-rich surface ($\rho = 0.4$) does not exhibit considerable modifications compared to the spectrum of the smooth surfaces. This indicates that the perturbation of the band structure induced by our rather gentle sputtering procedure is negligible. Two representative oxidation stages have been chosen to identify changes in the valence band regions of the smooth and defect-rich surfaces due to oxygen incorporation. The first stage results in a saturation of state α (10^8 L at 475 K[9]), whereas the second one (10^{11} L at 475 K) leads to the formation of the β peak as observed in the corresponding O_2 TD spectra. Figure 4 illustrates the modifications of the UPS-based valence band as induced by applying these two oxidation procedures. The lower left panel shows the smooth surface exposed to 10^8 L of oxygen. It exhibits two very pronounced

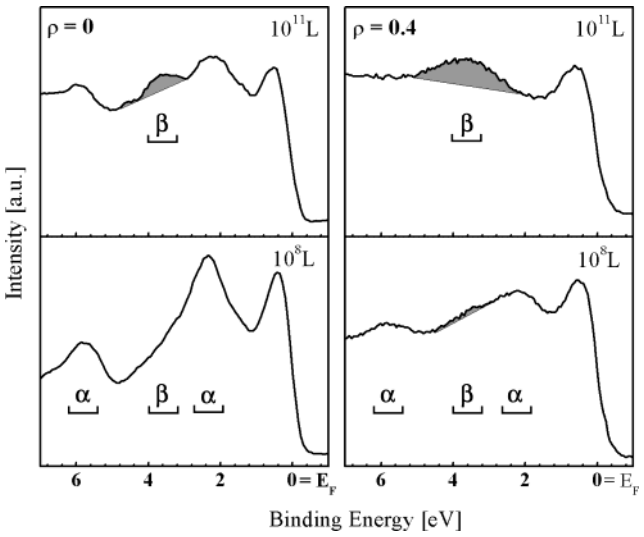

Figure 4. Left panel: evolution of the UPS-based valence band of a smooth surface, $\rho = 0$, as induced by exposing it to 10^8 L (bottom) and 10^{11} L (top) of oxygen. Right panel: modifications of the valence band by the same procedure applied to a defect-rich surface ($\rho = 0.4$; bottom, 10^8 L; top, 10^{11} L). In both cases the sample was exposed to oxygen at a surface temperature of 475 K.

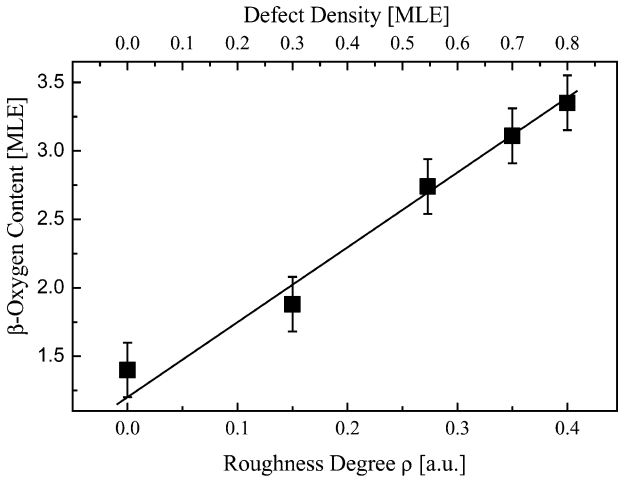

Figure 5. Oxygen load achieved via defects when surfaces differing by their mean roughness ρ were exposed to an oxygen amount of 10^8 L at a constant sample temperature of 575 K. The roughness scale has been expressed in units of the lateral density of defects by using related literature data (upper *x*-axis).[14]

peaks at 2.3 and 5.8 eV and only one weak shoulder at 3.6 eV. The peak shifts were recently assigned to the uptake of about 0.6 MLE of oxygen between the two outermost Ru layers, Ru(I) and Ru(II).[9] This is also mirrored by the O_2 TD spectra shown in Figure 2a. The spectrum of a smooth surface exposed to 10^{11} L (upper left panel) shows all three features as well-shaped peaks with the pronounced peak at 3.6 eV and consequently reflects the fact that in addition to state α another oxygen species constitutes state β. According to the TD spectrum taken after an exposure of 10^8 L, the sputtered surface should exhibit the nearly saturated α phase, $C_\alpha \approx 0.5$ MLE, and a small amount of species β. In the corresponding UP spectra already all three peaks are apparent (lower right panel). A well-shaped peak at 2.3 eV and a significantly shifted peak at 5.8 eV are visible. In comparison with its feature of a smooth surface, the peak at the binding energy of 3.6 eV is considerably more pronounced, reflecting the increased amount of defect-mediated oxygen phase. For exposures around 10^{11} L the surface contains a large amount of species β ($C_\beta \approx 4.5$ MLE) and a rather unchanged α phase. The corresponding UP spectrum however exhibits only one broad peak centered at 3.6 eV (upper right panel). It has to be noted that all the spectra presented do not exhibit the well-known spectral features characteristic for the bulk RuO_2 phase.[23] There, three characteristic peaks centered at 3.3, 4.5, and 7.2 eV form a rather broad structured band which is evidently absent in the spectra representing the dissolved oxygen phases. Thus, all presented data allow the peak at 3.6 eV to be identified as representing a novel oxygen species associated with incorporation through defects (TD-based state β). The peaks at binding energies of 2.3 and 5.8 eV can be related to oxygen atoms occupying the interlayer space beneath the smooth, nondefected areas of the surface, α.[9] Unfortunately, without advanced DFT calculation it remains unclear whether peak β results from the O 2p state or rather from the Ru band shifted due to the oxygen atoms in the vicinity of a defect.

To stress the role of defects in oxygen incorporation, we verified the relationship between the capacity of the surface defects toward oxygen storage and the mean surface roughness ρ. Figure 5 shows how the oxygen load C_β deposited in a defect-rich surface depends on the mean roughness ρ. This representative curve has been obtained by exposing the surfaces to an oxygen dose of 10^8 L at a sample temperature of 575 K followed by fitting and subsequent integration of Gaussian profiles representing peaks α and β. For soft sputtering conditions chosen here a linear dependence $C_\beta(\rho)$ has been found. Under the exposure conditions applied the oxygen content increases from 1.4 MLEs at a smooth surface up to 3.35 MLEs measured for a sputtered surface ($\rho = 0.4$). Thus, this simple experiment shows that the intentionally created surface defects raise the overall probability for oxygen incorporation. When the model of a sputtered surface as described in section B is accepted, the oxygen load, C_β, can be related to the total number of surface defects (top axis in Figure 4) and the mean capacity of an individual surface defect toward oxygen incorporation, $\chi = C_\beta / C_{\text{def}}$, can be derived. In the case presented here, nearly four oxygen atoms have been incorporated via a single surface defect (Ru vacancy). Obviously χ values increase with the oxygen dose applied.

Figure 6a shows several O_2 TD spectra taken after defect-rich surfaces kept at different temperatures were exposed to the same oxygen dose of 10^{11} L. The initial roughness of the sputtered surface was 0.4 in all experiments. The increasing preparation temperature raises the total oxygen content as reflected by the growth of both peaks α and β. However, the defect-assisted peak β becomes clearly distinguishable from other spectral features only for oxidation temperatures somewhere between 340 and 450 K. Figure 6b shows the total oxygen content, $C_{\text{total}}(T)$, and the defect-associated oxygen content, $C_\beta(T)$, obtained by fitting of the related regions of the O_2 TD spectra shown in Figure 6a by Gaussian profiles and integrating the resulting fits. Both $C_{\text{total}}(T)$ and $C_\beta(T)$ resemble rather a proportionality than an exponential behavior (▲ and ○, respectively). As shown in Figure 1 within the temperature range 400−600 K the defect-rich surface is partly repaired due to the progressing annealing process. In fact, the temperature dependence measured here represents a rather complex convolution of the two competing processes: the annihilation of defects due to thermal annealing and the defect-mediated oxygen incorporation. Using the He scattering data shown in Figure 1, we can roughly estimate the corresponding reduction of the initial defect density. The roughness still remaining at 585 K levels off around 0.25, which corresponds to a defect density of 0.45 MLE. In this case the oxygen load associated with peak β (Figure 6b)

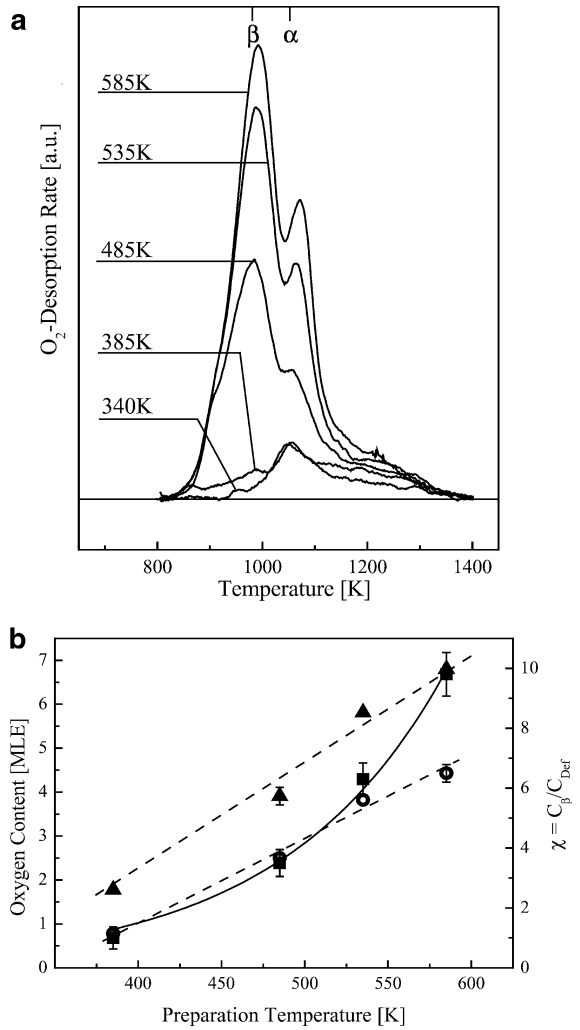

Figure 6. (a) O_2 TD spectra taken after exposure of the defect-rich surface to an oxygen amount of 10^{11} L at different sample temperatures as indicated. (b, bottom) The resulting oxygen content versus oxidation temperature (▲). Open circles represent the oxygen load deposited via channel β as a function of the sample temperature (○), $C_\beta(T_R)$. The solid line represents the corresponding capacity of an individual surface defect to accumulate oxygen. This curve was determined by dividing the resulting oxygen content $C_\beta(T_R)$ by the net defect density C_{def}.

reaches a value of 4.45 MLEs, which gives a number of about 9.9 oxygen atoms incorporated via an active defect. Following the same track for the lowest oxidation temperature, 385 K, where the annihilation is still not active, the corresponding defect capacity does not exceed 1.25 oxygen atoms per defect. The solid line (Figure 6b) illustrates how the defect capacity $\chi = C_\beta/C_{def}$ depends on the surface temperature. This function resembles an exponential curve that allows the Arrhenius procedure to be applied and the apparent activation energy to be roughly estimated for the defect-mediated oxygen incorporation. The best fit of this curve reveals a value $E(\beta) = 0.15$ eV, which is nearly 3 times lower than the apparent activation energy found for the high-temperature oxygen incorporation resulting in bulk oxides.[11] This comparison implies that the defect-mediated oxygen incorporation must play an important role also at the high-temperature oxidation regime as an efficient process foregoing oxide formation. This is supported by results recently obtained by high-resolution scanning X-ray photoelectron spectroscopy (XPS) applied to smooth and defect-rich surfaces at various sample temperatures up to 625 K.[25] The number of nearly 10 oxygen atoms associated with a single surface defect can be taken here as the upper limit achievable when only the

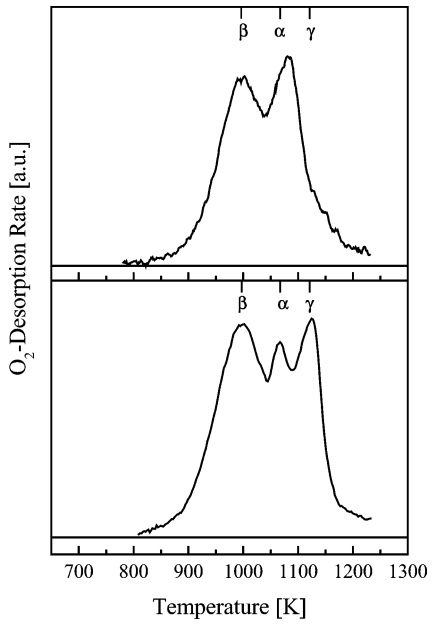

Figure 7. A comparison of two O_2 TD spectra taken after application of the same oxidation procedure to a defect-rich surface (upper panel) and a smooth surface (lower panel). Oxidation conditions: $T_R = 500$ K, oxygen dose 10^{13} L at a partial oxygen pressure of 1 bar. The mean roughness of the first sample was 0.4 measured by He scattering.

low-temperature oxidation regime is applied, which as known does not allow the formation of bulk oxides to occur ($T < 600$ K, $D < 10^{11}$ L).

Oxide-free oxygen incorporation into a smooth surface has been found to be limited first at very large oxygen exposures by the gradual formation of an oxide precursor which announces the formation of RuO_2 nuclei.[9] Such a state manifests itself by a well-shaped peak in O_2 TD spectra at 1120 K, there named γ, which coincides with the thermal decomposition of RuO_2 accompanied by the emission of RuO_3 molecules.[26] The latter phenomenon has been often used as a messenger for the presence of the bulk RuO_2 phase.[27] Note that this new feature does not represent bulk RuO_2 as formed in the high-temperature oxidation regime.[26,28] Bulk oxides are represented by a broad and less textured desorption band appearing between 800 and 1200 K resembling rather an overall envelope of all three peaks without any recognizable traces of sharp peaks.[26] Recent density functional theory (DFT)-based calculations predict the existence of a sandwich composed of a double of three oxygen layers intercalated into the two outermost Ru layers, $O_{ad}-Ru(I)-O-O-Ru(II)-O-Ru(III)$, as a metastable precursor for the final creation of bulk oxides.[21,22] In all TD spectra which exhibit a well-distinguishable γ peak the sum of the peak intensities, $I_\alpha + I_\beta + I_\gamma$, has been found to be about 4 MLEs. Consequently, peak γ signals the completion of the three-layer precursor phase, which presumably becomes transferred into oxide grains during TDS.

Figure 7 shows two O_2 TD spectra taken after the same oxygen treatment ($D = 10^{13}$ L, $T = 500$ K) was applied to a smooth and a defect-rich surface, lower and upper panels, respectively. The desorption spectrum taken from a smooth surface exhibits three well-recognizable peaks. In addition to the well-known peaks of the subsurface- and the defect-mediated oxygen, α and β peaks, the third peak γ arises around 1120 K. In contrast, the spectrum taken after oxygen exposure to a defect-rich surface ($\rho = 0.4$) exhibits only α and β peaks with a small shoulder on the high-temperature side which indicates traces of peak γ. This comparison points to a hindrance of the

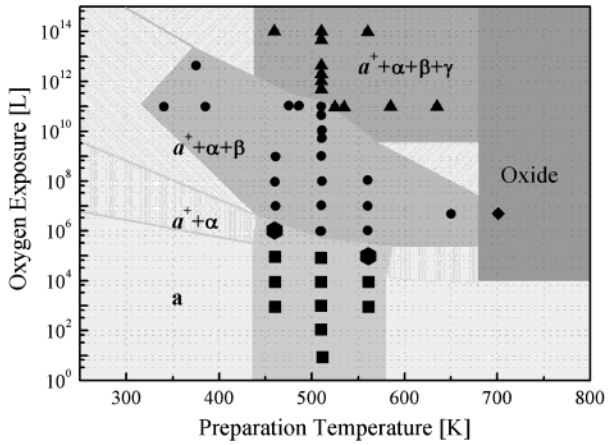

Figure 8. State diagram for oxygen incorporation into a defect-rich Ru(0001) surface ($\rho = 0.4$). See the text for details. It defines the area in the exposure−temperature space where oxygen incorporation into a sputtered surface proceeds without the formation of bulk oxides.

formation of oxide precursors on a larger scale due to surface defects. In fact, peak γ appears also for defect-rich surfaces but at significantly larger oxygen exposures and higher preparation temperatures, i.e., T_γ(smooth) < T_γ(rough) for the same oxygen exposure.

C. State Diagram of Defect-Mediated Oxygen Incorporation. Figure 8 shows a state diagram for oxygen incorporation based on the TDS, TEAS, and UPS studies presented above. It summarizes the findings discussed above and defines the exposure−temperature space, $D-T$, where special O_2 TD features signal the presence of well-defined oxygen species or a coexistence of different species. The distinguishable states are marked by different gray areas. Different geometric symbols mark the location of experiments which revealed the characteristic and well-distinguishable TD features. In the lower part of this diagram, $D < 5 \times 10^5$ L, only the adsorbed oxygen phase could be achieved (a in Figure 8). Within the whole temperature region the formation of a saturated adlayer appeared for exposures between 1×10^4 and 5×10^5 L. For slightly higher exposures the TD spectra exhibit the sharp peak α growing out from the broad band representing the adsorbed phase. It signals that a new process starts, the occupation of the subsurface region beneath smooth surface areas covered by a 1×1-O adlayer. Predominantly the interlayer space between Ru(I) and Ru(II) is occupied. These two peaks remain the only TD features within a rather narrow strip, from $(1-2) \times 10^5$ L at 575 K to 5×10^5 to 10^7 L at 350 K (●). It has to be noted that at this oxidation stage the oxygen adlayer, 1×1-O, is considerably modified by oxygen atoms occupying the interlayer space, denoted here as a^+. This distinction is according to a recent scanning XPS-based study which revealed clearly separated Ru 3d spectral features for the 1×1-O adlayer with and without oxygen atoms beneath.[29] For higher oxygen exposures the corresponding TD spectra show three coexisting features simultaneously, a^+, α, and β (●). This state covers the large central part of this diagram. It reveals that in addition to channel α oxygen incorporation via surface defects is active and at higher temperatures represents the dominating channel. The central area is limited by a rather well-defined narrow borderline around $T \approx 650$ K which at its right flank signals the formation of bulk oxides (◆). O_2 TD spectra of surfaces containing bulk oxides exhibit a very intense and wide TD band.[27] For lower temperatures and higher exposures, $D > 10^{10}$ to 10^{14} L, the central area is limited by the appearance of peak γ (▲). The upper left corner of this diagram is not covered by corresponding experimental points, $T < 350$ K and $D > 10^{12}$ L. It seems that peak γ may appear only at considerably higher exposures, which might extend the region for oxide-free oxygen incorporation. We plan to perform exposure experiments at oxygen pressures up to 100 bar to evaluate this low-temperature oxygen dissolution. Within the high-temperature side, $T > 650$ K, only moderate-pressure experiments ($p < 20$ mbar) could be conducted because our experimental setup appeared insufficient to ensure well-defined oxidation conditions when the hot sample was exposed to oxygen at a partial pressure of 1 bar.

4. Discussion

We focus here on some aspects concerning the physical model of surface-defect-mediated oxygen dissolution. As mentioned above, oxygen incorporation through channel β already becomes significant when the occupation of the subsurface region via channel α stagnates. It is dominating when the capacity of channel α saturates. Such a relationship implies a strong competition between the two possible channels. This finding can be explained by considering a kinetic hindrance of channel α due to a reduced probability for diffusion of oxygen molecules as occurring when in addition to the outermost adlayer also the interlayer space becomes occupied by oxygen atoms. In such a situation the accessibility of Ru atoms not surrounded by oxygen drops considerably. Ru(II) atoms are practically not accessible for oxygen due to a shielding $O_{ad}-Ru(I)-O_{sub}$ sandwich above. Thus, oxygen incorporation via channel α slows drastically. The only remaining channel where the oxygen incorporation may still take place is a Ru vacancy. At the current stage the question why an individual vacancy exhibits a still high ability to convert oxygen from the surface to beneath the surface even after an exposure of 10^{11} L can be answered only tentatively. One might speculate that a Ru vacancy induces a local reconstruction in the surrounding Ru lattice, which consequently makes the oxygen transport from the vacancy site into the subsurface more likely even at low sample temperatures.

As estimated from the temperature dependence of C_β, a surface defect becomes inactive after the incorporation of 9−10 oxygen atoms. After this step the overall ability of the whole surface to accumulate oxygen tends to that exhibited by the smooth surface, where only the rather inefficient channel α remains active. Obviously, at this stage only speculative ideas concerning the limited capacity of defects can be proposed. Nevertheless, it seems plausible that defects enable oxygen to outflank the path of oxygen incorporation via channel α presumably by making the deeper layers Ru(II), Ru(III), and, potentially, Ru(IV) accessible for oxygen. This lateral method of oxygen incorporation may ensure the population of subsurface regions of the defect-free surface areas, which remain well-shielded by the $O_{ad}-Ru(I)-O$ trilayer on the top.[21,22] Consequently, the hindrance responsible for the characteristic slowing of the incorporation path α may be bypassed. Thus, a Ru vacancy in the Ru(II) layer might act as a key opening a new lateral channel for a side-path oxygen incorporation into the interlayer space, Ru(II)−Ru(III), as well as for the penetration of adjacent Ru(IV). According to the recent DFT-based model of oxygen incorporation into the subsurface, each outermost Ru layer is capable of binding nearly 2 MLEs of oxygen.[22,23] Thus, such a scenario implies an upper limit of the surface capacity for oxygen storage to be around 8 MLEs, which nicely matches the experimental finding.

The TDS-based analysis revealed that surface defects not only represent centers for desorption of the accumulated oxygen but also act as efficient channels for oxygen incorporation into the

subsurface region. The UP spectra of the sputtered and oxidized surfaces add another aspect of the defect-mediated phase. They show that the oxygen incorporated into the subsurface via defects exhibits a well-defined electronic feature (peak at 3.6 eV). A plausible explanation of this feature might be gained by postulating that the related oxygen species can be distinguished by its location in certain regions of the subsurface. Support for this concept can be found in the DFT-based valence-band DOS calculations as performed for oxygen incorporation in a smooth surface.[22,23] The calculations mirror the 4d DOS of a decoupled trilayer, $O_{ad}-Ru(I)-O---O-Ru(II)-Ru(III)$, corresponding to a saturated α phase followed by the initial occupation stage of deeper lying Ru layers by oxygen (see Figure 4, lower left panel). According to our model postulated above, the occupation of the interlayer spaces Ru(I)−Ru(II) and Ru(II)−Ru(III) beneath the defect-free areas might proceed more efficiently via surface defects. In this sense the decoupling of the trilayer, $O_{ad}-Ru(I)-O$, starting when the Ru(II)−Ru(III) layers are increasingly populated by oxygen atoms, may be considered as resulting mainly from the presence of surface defects. Consequently, the valence band spectra of such a decoupled trilayer should exhibit spectral features stemmed from state β, too. The calculated 4d DOS displays three peaks, a broad feature between 5.6 and 6.4 eV and two weak peaks centered at 3.4 and 1.8 eV.[22,23] These binding energies are all observed for peaks in the measured spectra as well though the measured intensities are different. However, the theory mirrors rather satisfactorily the main trend associated with the formation of α and β phases. Note, however, that the model does not include contributions of the Ru(II) layer to the overall 4d DOS. A better agreement of the model and experimental peak positions is expected by including all adequately weighted contributions from the Ru(II) and Ru(III) layers in the calculations. Thus, at the moment we can only postulate that the wide peak β at 3.6 eV can be assigned to oxygen atoms located between the deeper lying Ru layers, Ru(II), Ru(III), and Ru(IV). These subsurface regions are only scarcely accessible for oxygen passing through the smooth and defect-free areas of the topmost layers; they become easily accessible for oxygen only via surface defects.

When a possible practical application of oxygen dissolution was considered, it became evident that the LTHP oxidation regime can be purposefully used for storage of atomic oxygen at sputtered Ru(0001) surfaces. Stored oxygen can be removed simply by heating as well as by exposing the sample to CO flux. Such incorporation−removal cycles can be repeated to find significant reaction-induced surface modifications or some reaction remainders. However, the efficiency of this storage method is rather poor. Under a partial oxygen pressure of 1 bar it takes about 1 day to deposit nearly 10 oxygen monolayers; i.e., the overall storage efficiency does not override a level of 3.6×10^{11} atoms/(cm^2 s). In addition, the maximum capacity of the surface toward oxide-free oxygen incorporation remains below 10 MLEs. It remains to make an educated guess that by increasing the partial oxygen pressure up to about 100 bar the maximum capacity might be higher.

5. Summary

Intentionally created surface defects raise the capacity of Ru(0001) for oxygen incorporation when the LTHP oxidation procedure is applied. The oxygen phase incorporated via surface defects manifests itself by a peak in the O_2 TD spectrum at 940 K as well as in valence band UPS by a peak at $E_B = 3.6$ eV. Defect-mediated oxygen incorporation represents a thermally activated process characterized by an apparent activation barrier of 0.15 eV, which is considerably lower than that found for oxygen incorporation by oxide formation. Under the LTHP conditions applied here an individual defect is capable of accumulating nearly 10 oxygen atoms. The state diagram for defect-mediated oxygen incorporation indicates that this process is only limited by the formation of an oxide precursor phase for large oxygen exposures on one side, as well as by the formation of bulk oxides at high temperatures on the other.

Acknowledgment. We appreciate M. Scheffler and K. Reuter from FHI in Berlin for very interesting discussions. R.B. and H.N. appreciate the financial support of the Deutsche Forschungsgemeinschaft (Project Ni-451). A.B. thanks Gerhard Ertl for initializing and supporting the long-term project concerning the study of oxidation-based phenomena on Ru(0001).

References and Notes

(1) Bonnell, D. A. *Scanning probe microscopy and spectroscopy: theory, techniques and applications*, 2nd ed.; Wiley-VCH: New York, 2000.
(2) Fauth, K.; Hessler, M.; Batchelor, D.; Schütz, G. *Surf. Sci*. **2003**, *529*, 397.
(3) Häkkinen, K.; Manninen, M. *J. Chem. Phys.* **1996**, *105*, 10565.
(4) Abbet, S.; Riedo, E.; Brune, H.; Heiz, U.; Ferrari, A. M.; Giordano, L.; Pacchioni, G. *J. Am. Chem. Soc.* **2001**, *123*, 6172.
(5) Holloway, S. *Surf. Sci.* **2003**, *540*, 1.
(6) Hirsimäki, M.; Chorkendorff, I. *Surf. Sci.* **2003**, *538*, 233.
(7) Sonnet, Ph.; Stauffer, L.; Selloni, A.; Kelires, P. C. *Surf. Sci.* **2003**, *544*, 277.
(8) (a) Bedrane, S.; Descorme, C.; Duprez, D. *Catal. Today* **2002**, *75*, 401. (b) Bedrane, S.; Descorme, C.; Duprez, D. *Catal. Today* **2002**, *73*, 233.
(9) Blume, R.; Niehus, H.; Conrad, H.; Böttcher, A. *J. Chem. Phys*. **2004**, *120*, 3871.
(10) Poelsema, B.; Comsa, G. *Scattering of Thermal Energy Atoms from Disordered Surfaces, Springer Tracts in Modern Physics*; Springer-Verlag: Berlin, 1989; Vol. 15.
(11) Böttcher, A.; Niehus, H. *J. Chem. Phys.* **1999**, *110*, 3186.
(12) Surnev, I.; Rangelov, G.; Bliznakov, G. *Surf. Sci*. **1985**, *159*, 299.
(13) Madey, T. E.; Engelhardt, H. A.; Menzel, D. *Surf. Sci.* **1975**, *48*, 304.
(14) Burnett, J. W.; Biersack, J. P.; Gruen, D. M.; Jorgensen, B.; Krauss, A. R.; Pellin, M. J.; Schweitzer, E. L.; Yates, J. T.; Young, C. E. *J. Vac. Sci. Technol., A* **1988**, *6*, 2064.
(15) Burnett, J. W.; Pellin, M. J.; Calaway, W. F.; Gruen, D. M. *Phys. Rev. Lett.* **1989**, *63*, 562.
(16) Yamamura, Y.; Tawara, H. *At. Data Nucl. Data Tables* **1996**, *62*, 149.
(17) Beeby, J. L. *J. Phys. C* **1971**, *4*, L395.
(18) Lombardo, S. J.; Bell, A. T. *Surf. Sci. Rep*. **1991**, *13*, 1.
(19) Stampfl, C.; Kreutzer, H. J.; Payne, S. H.; Pfnür, H.; Scheffler, M. *Phys. Rev. Lett*. **1999**, *83*, 2993.
(20) Stampfl, C.; Schwegmann, S.; Over, H.; Scheffler, M.; Ertl, G. *Phys. Rev. Lett.* **1996**, *77*, 3371.
(21) Reuter, K.; Stampfl, C.; Ganduglia-Pirovano, M. V.; Scheffler, M. *Chem. Phys. Lett.* **2002**, *352*, 311.
(22) Reuter, K.; Ganduglia-Pirovano, M. V.; Stampfl, C.; Scheffler, M. *Phys. Rev. B* **2002**, *65*, 165403.
(23) Böttcher, A.; Niehus, H. *Phys. Rev. B* **1999**, *60*, 14396.
(24) Pelzer, T.; Ceballos, G.; Zbikowski, F.; Willerding, B.; Wandelt, K.; Thomann, U.; Reuss, Ch.; Fauster, Th.; Braun, J. *J. Phys.: Condens. Matter* **2000**, *12*, 2193.
(25) Blume, R.; Niehus, H.; Conrad, H.; Böttcher, A. Manuscript in preparation.
(26) Böttcher, A.; Conrad, H.; Niehus, H. *J. Chem. Phys.* **2000**, *112*, 4779.
(27) Malik, I. J.; Hrbek, J. *J. Vac. Sci. Technol., A* **1992**, *10*, 2565.
(28) Over, H.; Kim, Y. D.; Seitsonen, A. P.; Wendt, S.; Lundgren, E.; Schmid, M.; Varga, P.; Morgante, A.; Ertl, G. *Science* **2000**, *287*, 1474.
(29) Böttcher, A.; Starke, U.; Conrad, H.; Blume, R.; Gregoriatti, L.; Kaulich, V.; Barinov, A.; Kiskinova, M. *J. Chem. Phys.* **2002**, *117*, 8104.
(30) Böttcher, A.; Niehus, H.; Schwegmann, S.; Over, H.; Ertl, G. *J. Phys. Chem. B* **1997**, *1001*, 11185.